

Comparison of Elastic and Corrosion Behaviour of Sintered Iron Before and After Its Long Time Immersion in Hank's Solution

Miriam Kupková^{1,*}, Martin Kupka², Monika Hrubovčáková¹

¹Institute of Materials Research, Slovak Academy of Sciences, Watsonova 47, SK-040 01 Košice, Slovak Republic

²Institute of Experimental Physics, Slovak Academy of Sciences, Watsonova 47, SK-040 01 Košice, Slovak Republic

*E-mail: mkupkova@imr.saske.sk

Received: 27 December 2016 / *Accepted:* 6 February 2017 / *Published:* 12 March 2017

Test bars were prepared from an iron powder by pressing and sintering. Sintered bars exhibited porosity between 15 and 40%. Because of their shape and volume fraction, the pores were expected to form a continuous inter-connected bar-spanning structure. Effective Young's modulus, determined from the frequency of flexural vibration of each bar, increased with decreasing porosity. When brought into contact with Hank's solution, the bars took up corrosion potentials which increased with decreasing porosity. A possible cause was that the external face of a bar (cathode) and internal pore walls (anode) formed a galvanic couple, and the cathode-to-anode area ratio increased with decreasing porosity. After eight weeks of immersion in Hank's solution, each of bars was found heavier as in as-sintered state, and the weight gain was proportional to the internal surface of the bar. The effective Young's modulus was higher than that of as-sintered material. The corrosion potential was practically independent on porosity. The most likely cause of such a behaviour was a layer of corrosion products covering nearly uniformly almost entire internal surface of a bar. The corrosion/reaction products increased the mass of a bar, enhanced its stiffness in compression, and altered the character of corrosion.

Keywords: sintered Fe materials, porous electrodes, corrosion, Hank's solution, Young's modulus

1. INTRODUCTION

People have made useful things from metallic powders throughout the ages. Today's powder-forming routes are, as is commonly believed, superior to their predecessors in all aspects, especially in versatility and productivity. There is a wide spectrum of engineering components mass-produced from

powdered metals which are applied in aeroplanes, cars, consumer electronics, etc. [1]. The powder metallurgy is also used for fabricating various medical devices which can save the human life and/or improve its quality.

To do their job well, the devices have to be made from materials which meet specific mechanical and chemical requirements. For example, permanent implants, such as hip and knee joints, are expected to be highly resistant to corrosion and to possess mechanical stiffness similar to that of bone, while prospective temporary implants, such as coronary stents, are expected to corrode at a rate that match the rate at which the tissue heals and regenerates, and to maintain mechanical integrity until the surrounding tissue becomes able to resist acted loads itself.

Until special procedures are used, sintered metals are inherently porous. The current knowledge concerning corrosion behaviour of such porous bodies is mostly based on results from simple immersion tests in quite simple electrolytes such as acids and neutral saline solutions [2-4]. Less effort was put into investigation of corrosion of porous bodies in more complex electrolytes which are capable of forming insoluble precipitates.

The changes in mechanical properties with proceeding corrosion were not studied very extensively, too (e.g. [5]).

This article reports on preliminary results concerning changes in corrosion parameters and effective Young's modulus of a sintered iron (a prospective material for temporary coronary stents or synthetic scaffolds for bone tissue engineering) caused by its long-term exposure to Hank's solution (an electrolyte simulating body fluids).

2. MATERIALS AND METHODS

To simulate the internal environment of the human body, Hank's solution maintained at a temperature of 37°C was used as an electrolyte in all experiments reported in this article. The solution was composed of (in g/l) 8.00 NaCl, 1.00 Glucose, 0.60 KH₂PO₄, 0.40 KCl, 0.35 NaHCO₃, 0.14 CaCl₂, 0.10 MgCl₂ 6H₂O, 0.06 MgSO₄ 7H₂O, and 0.06 NaH₂PO₄ 2H₂O with a pH value of 7.4.

Water-atomized iron powder, Höganäs ASC 100.29 grade, was pressed to prismatic bars (20mm × 4mm × 4mm) in a die under compaction pressures of 100, 200, 400 and 600 MPa. No lubricant was used.

Next, green compacts underwent a thermal treatment. They were held at the sintering temperature of 1120°C in a laboratory furnace Carbolyte for 60 minutes. The furnace was heated up and cooled down at a rate of 10°C/min. The processing atmosphere consisted of H₂ and flowed at a rate of 4 l/min.

Density of sintered compacts was obtained by weighing the compacts and measuring their dimensions.

Samples intended for immersion tests were subjected to the ultrasonic cleaning in acetone and ethanol for 10 min each. Clean samples were immersed in 50 ml of Hank's solution. After 8 weeks, the corroded samples were taken out of the solution and were ultrasonically cleaned in distilled water and ethanol for 10 min each, air dried and weighed.

The microstructures of samples and the composition of corrosion products formed during the long time corrosion were determined by SEM with EDX analysis.

Some mechanical and electrochemical properties of samples were investigated both in as-sintered state and in after-exposure state.

Potentiodynamic polarization measurements were carried out in a conventional three-electrode setup with the potentiostat PARSTAD 4000. A saturated calomel electrode (SCE) was used as the reference electrode, platinum acted as a counter electrode. About 1 cm^2 of the surface of sintered iron sample was exposed to the electrolyte and acted as a working electrode. The samples were kept immersed in the electrolyte for 2 hour before the polarization curves were recorded. During the measurement, the potential varied from $E_{\text{corr}}-250 \text{ mV}$ to $E_{\text{corr}}+250 \text{ mV}$ at a rate of 0.16 mV/s .

The modulus of elasticity was determined by a dynamic method. The natural frequency of the fundamental bending mode was measured by means of BUZZOSONIC 5.9.6, USA. The corresponding bending stiffness was evaluated for each of bars. For a macroscopically homogeneous bar, the bending stiffness reduces to the product $Y_{\text{eff}}I$, where Y_{eff} is the effective Young's modulus of a material of which the bar is made and I is the area moment of inertia of the bar cross section. If the bar is macroscopically heterogeneous, the bending stiffness is connected with material properties and geometric characteristics in a more complex way.

3. RESULTS AND DISCUSSION

3.1 Static immersion tests

Sintered materials are inherently porous. Void spaces in a sintered body reduce the load-bearing cross section and enlarge the metal - environment interfacial area, which alters the mechanical and electrochemical behaviour of the body.

The relative density ρ/ρ_0 is one of important parameters which governs almost all properties of sintered materials. In this ratio, ρ is the density of the sintered material and usually increases with increasing compaction pressure (Tab. 1), and ρ_0 is the density of the solid matrix.

Table 1. Densities of studied sintered iron materials.

Compaction pressure [MPa]	Density, ρ [$\text{g}\cdot\text{cm}^{-3}$]	Relative density, ρ/ρ_0
100	4.85 ± 0.12	0.616 ± 0.015
200	5.49 ± 0.10	0.697 ± 0.013
400	6.28 ± 0.09	0.798 ± 0.011
600	6.72 ± 0.04	0.853 ± 0.005

An internal surface area, i.e. the surface area of the pore walls, is usually large compared to the exterior geometric surface area of a sintered body. A simple expression which relates the internal surface area per unit volume, S_V , and the relative density of sintered material reads [6].

$$S_V = \text{constant} \times \left[\left(\frac{\rho}{\rho_0} \right)^{2/3} - \left(\frac{\rho}{\rho_0} \right) \right] \tag{1}$$

The constant of proportionality depends, among other things, on the size of sintered particles and on the mean number of interparticle contacts for each particle.

A large internal surface area plays an important role in the corrosion behaviour of sintered materials. More precisely, the area of internal surface which is accessible to the electrolyte.

In theoretical investigation of permeability of porous materials, real materials are idealized as a continuous solid matrix with randomly created identical convex cavities. If the volume fraction occupied by a solid matrix falls below the value at which the overlapping pores first form a continuous path spanning the sample, the specimen becomes permeable.

The critical porosity, referred to as the percolation threshold, is about 30% for overlapping spherical pores [7]. If the spherical pores are replaced by oblate or prolate spheroids, the percolation threshold decreases. For disclike pores with the aspect ratio of about 0.1 or for needlelike pores with the aspect ratio of about 8-10, the critical porosity sufficient for the emergence of a continuous pore network crossing the sample is about 10% or less [7,8].

Taking into account the shape of pores and the total porosity of samples investigated, it is possible to assume that the most of pores are mutually interconnected.

If the whole sample is immersed in a solution for a long time, the solution manages to fill all accessible void spaces of the sample.

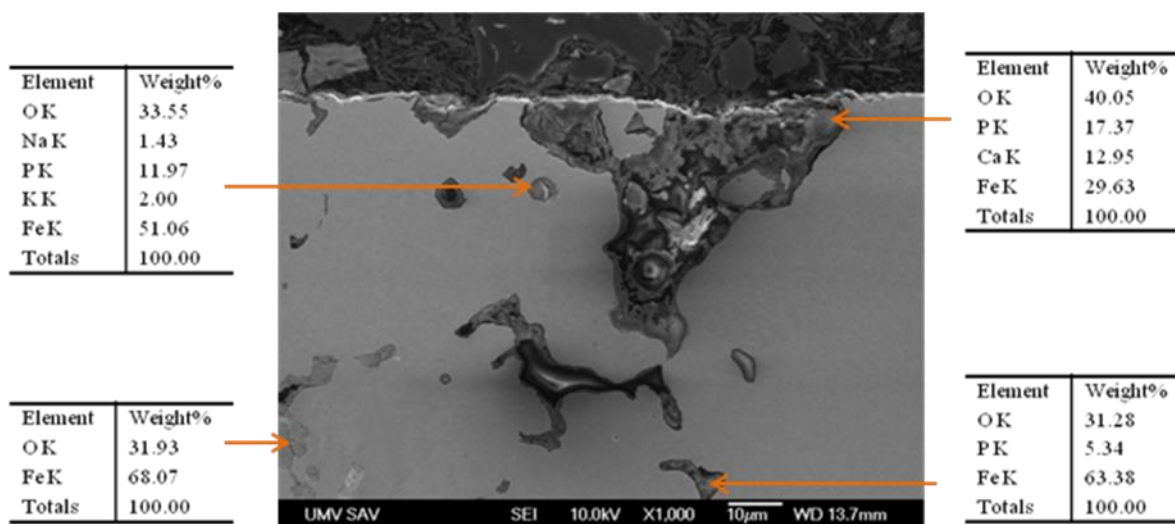


Figure 1. A SEM micrograph of a polished section of sintered iron compact after eight weeks of immersion in Hank's solution, and the EDX analysis of corrosion products. The presented sample was compacted under 600 MPa.

As the interaction of iron surface with Hank's solution proceeds, insoluble products of degradation can adhere to and accumulate on the corroding surface. The layer arising during this

process consists mainly of iron hydroxides and precipitated compounds of calcium and phosphorus (Fig. 1) [9,10]. These coats increase the mass of sample.

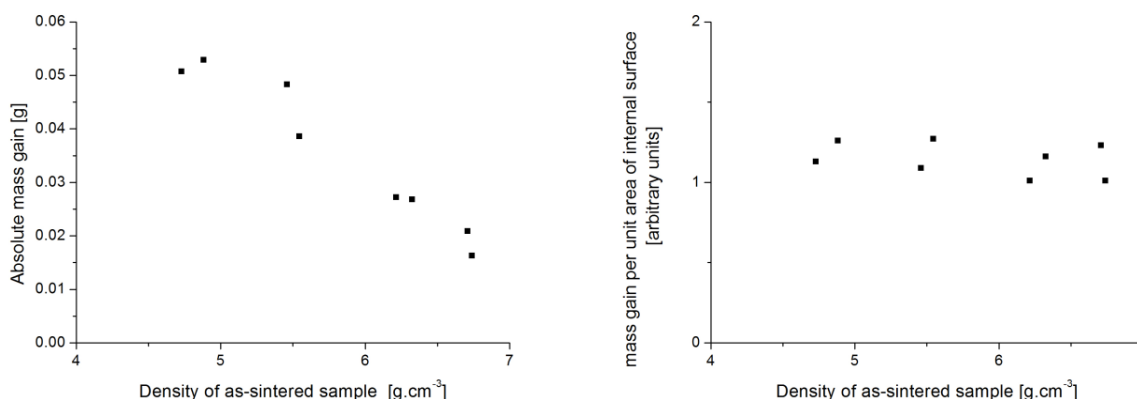


Figure 2. The increase in mass of sintered iron samples due to their eight-week immersion in Hank's solution. The figure shows the absolute mass gain on the left and mass gain per unit area of internal surface on the right.

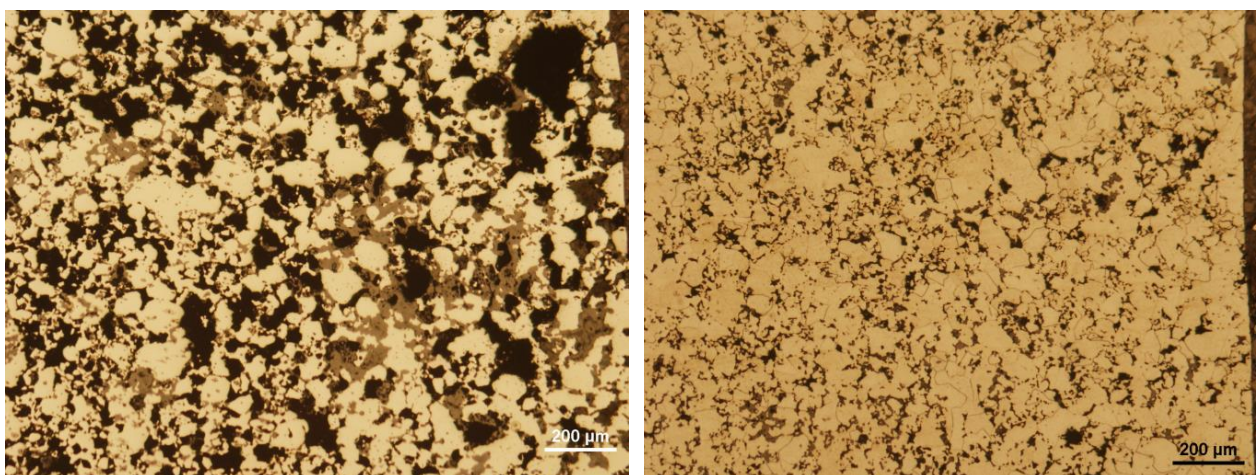


Figure 3. Optical micrographs of polished and etched sections through the interior of sintered Fe samples after eight weeks of immersion in Hank's solution. The figure shows the sample compacted at 100 MPa on the left and the sample compacted at 400 MPa on the right.

Fig. 2 shows the increase in mass of samples caused by their eight-week exposure to Hank's solution, and the increase in mass - to - geometric volume $\times [(\rho/\rho_0)^{2/3} - (\rho/\rho_0)]$ ratio. It can be seen that the mass enhancement of investigated samples is proportional to their initial internal surface area, that is,

$$\frac{\text{mass after immersion} - \text{mass before immersion}}{(\text{geometric volume}) \times (\text{internal surface area per unit volume})} = \text{const.} \tag{2}$$

A possible simple explanation is that the corroding internal surfaces of all samples were covered by nearly uniform layers of degradation products (Fig. 3). The composition and thickness of this layer are supposed to be nearly the same for all samples.

The formation of the layer of insoluble degradation products can slow down the dissolution of metallic ions and so can cause the degradation rate to decrease [9,10].

3.2 Potentiodynamic polarization measurements

Corrosion characteristics of both as-sintered samples and samples after eight-week exposure to Hank's solution were evaluated by the Tafel extrapolation technique applied to data obtained from potentiodynamic polarization measurements. As an electrolyte, Hank's solution was used.

Potentiodynamic polarisation tests provided relevant data on the basis of which the corresponding Tafel plots were constructed. Some of them are presented in Fig. 4. Current densities were evaluated by use of the electrode's geometric surface area exposed to the electrolyte. Anodic and cathodic Tafel regions of each Tafel plot were extrapolated back to their intersection, and the intersection point determined the corrosion potential, E_{corr} , and corrosion current density, i_{corr} . The values of E_{corr} , i_{corr} for the studied materials are listed in Tab. 2 for as-sintered samples and in Tab. 3 for samples after long term immersion in Hank's solution.

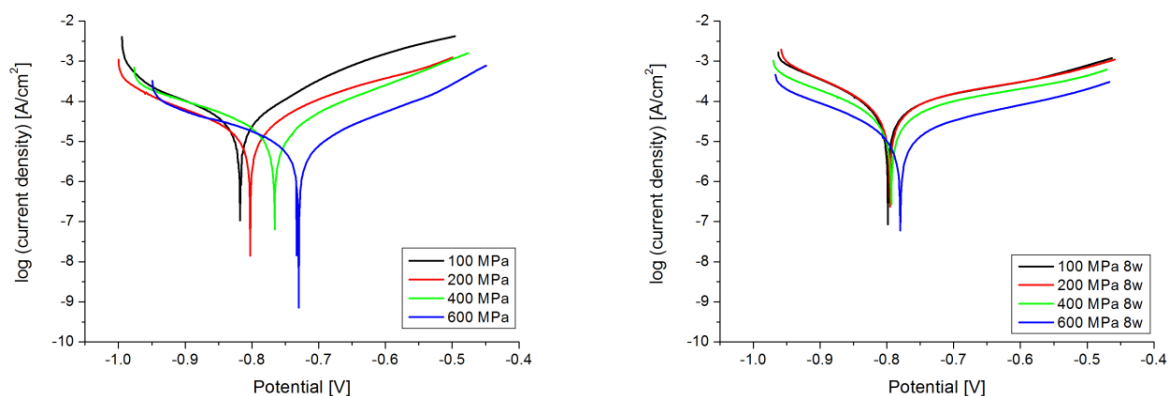


Figure 4. Tafel plots for sintered iron samples dipped into Hank's solution. The figure shows Tafel plots for as-sintered samples on the left and for samples underwent eight weeks of immersion in Hank's solution on the right.

Table 2. Corrosion parameters for as-sintered iron samples.

Compaction pressure [MPa]	i_{corr} [$\mu\text{A}/\text{cm}^2$]	E_{corr} [mV]	Tafel slope [mV/dec]	
			Cathodic	anodic
100	24.12	-818	176	129
200	14.94	-801	213	137
400	11.39	-764	169	139
600	4.40	-732	161	132

Table 3. Corrosion parameters for sintered iron samples after eight weeks of immersion in Hank's solution.

Compaction pressure [MPa]	i_{corr} [$\mu\text{A}/\text{cm}^2$]	E_{corr} [mV]	Tafel slope [mV/dec]	
			cathodic	anodic
100	39.81	-798	165	424
200	39.81	-795	193	468
400	25.12	-793	285	687
600	6.31	-780	237	477

It can be seen that the corrosion potential of as-sintered iron samples varies significantly with the sample density, while the corrosion potentials nearly equal each other for samples which underwent exposure to Hank's solution.

To gain insight into the behaviour of sintered iron or steel solids in contact with an electrolytic solution, a galvanic corrosion has often been taken into consideration. It is supposed that the outer and inner surfaces of the porous body are galvanically coupled (e.g. [3]). The free outer surface serves as the cathode and the surfaces of inner walls of pores act as the anode.

Assuming such a situation for a used electrode, the corrosion potential and corrosion current density are functions of areas of cathodic and anodic regions of the surface in contact with the electrolyte. For a simple situation E_{corr} and i_{corr} can be expressed as (e.g. [11])

$$E_{corr} = C_1 \log\left(\frac{A_{cathode}}{A_{anode}}\right) + C_2 \quad (3)$$

and

$$\log(i_{corr}) = \log\left(C_3 \frac{A_{anode}}{A_{geometric}}\right) + C_4 \log\left(\frac{A_{cathode}}{A_{anode}}\right) + C_5. \quad (4)$$

Here $A_{geometric}$ is the area of the exterior geometric surface of the electrode exposed to the electrolyte, $A_{cathode}$ is the real area of cathodic region and A_{anode} is the real area of anodic region of the electrode real surface (outer or inner) in contact with the electrolyte. Constants C_1, \dots, C_5 depend on corrosion potentials, corrosion current densities, Tafel slopes of "anode" and "cathode" materials alone.

For a material with randomly distributed pores, the "areal" porosity would numerically equal the "volumetric" porosity [12]. Therefore, the area fraction of the external face of electrode occupied by void regions is P and the area fraction occupied by solid regions is $1-P$. So, the area of cathode is proportional to $1-P$,

$$A_{cathode} = (1-P)A_{geometric} \quad (5)$$

The area of anode is proportional to the area of inner walls of pores which are in contact with the electrolyte. If the examined (not insulated) base of a prismatic electrode is shallowly dipped into electrolyte, the anode's area is

$$A_{anode} \propto S_V h A_{geometric} \tag{6}$$

Here S_V is the internal surface area per unit volume of sintered material and h is the dipping depth.

If the relative density of a porous sample is only slightly less than one, S_V gets proportional to porosity. So, for materials with a moderate porosity, expression (6) reduces to a simpler form

$$A_{anode} \propto P A_{geometric} \tag{7}$$

Experimental data on corrosion potentials and corrosion current densities of as-sintered materials as well as fits to these data by the use of functions (3) and (4) are presented in Fig. 5 and Fig. 6.

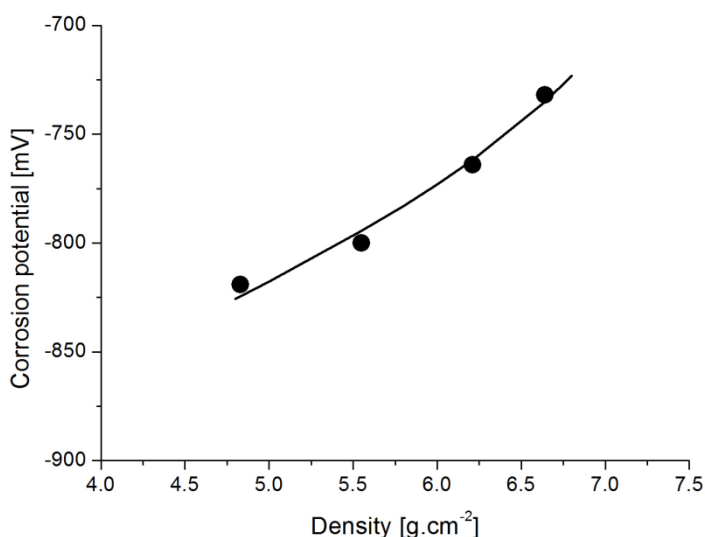


Figure 5. Corrosion potential of as-sintered iron sample in Hank's solution as a function of sample's density. Circles represent experimental data and the solid line is given by $E_{corr} = -962.94 + 184.98 \times \log(\rho/\rho_0) - 184.98 \times \log[(\rho/\rho_0)^{2/3} - (\rho/\rho_0)]$, in mV. This equation was determined by a regression analysis used to fit experimental data with the corrosion potential model represented by equations (3), (5), (6) and (1). Numerical parameters represent various combinations of model constants.

As regards the after-exposure materials, it looks like the presence of degradation products converts the initial galvanic corrosion (before exposure) into a general one (after exposure). The idea

that the corrosion became general is implied by the behaviour of corrosion potentials of after-exposure samples, which are of nearly equal value in spite of different porosities (Tab. 3).

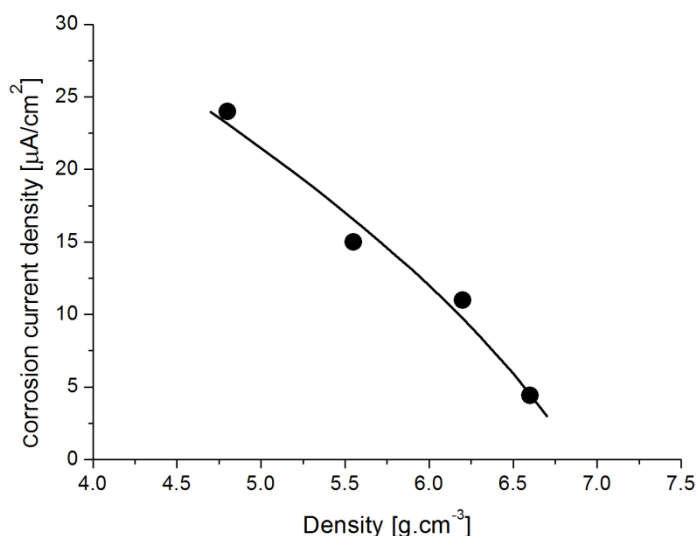


Figure 6. Corrosion current density of as-sintered iron sample in Hank's solution as a function of sample's density. Circles represent experimental data and the solid line is given by $\log(i_{corr}) = 3.17 - 1.01 \times \log(\rho/\rho_0) + 2.01 \times \log[(\rho/\rho_0)^{2/3} - (\rho/\rho_0)]$, in $\log(\mu\text{A}/\text{cm}^2)$. This equation was determined by a regression analysis used to fit experimental data with the corrosion current model represented by equations (4), (5), (6) and (1). Numerical parameters represent various combinations of model constants.

3.3 Dynamic measurements of effective Young's modulus

When probed with a submicron spatial resolution, the properties of sintered materials vary from point to point. That is, sintered materials are inhomogeneous at the microscopic level. But practically important material's properties are those which manifest themselves on "human" length scales, that is on scales which are large compared to any microstructure. There is theoretical and experimental evidence that the macroscopic mechanical response of real sintered body is equivalent to the response of an equally shaped and sized body made of hypothetical homogeneous material with the effective elastic constants.

The resistance of a material to elastic deformation is measured by the effective Young's modulus. This modulus is thus reflected in the speed of elastic waves propagating in a material and hence in natural frequencies of vibrations of macroscopic bodies. The modulus-determining methods are often based on the measurement of these frequencies.

When flexural vibrations of a bar-shaped sample are used for determining the modulus, the frequency of fundamental bending mode, the sample's dimensions and its mass are measured. Processing these experimental data provides one with the value of bending stiffness of a bar tested. The bending stiffness - to - area moment of inertia of the bar cross section ratio is termed the effective

Young's modulus, Y_{eff} . If the sample is made of an ordinary, homogeneous, linearly elastic material, this ratio indeed represents the material's Young's modulus [13].

The modulus of elasticity of each investigated material was determined in this way. Results are presented in Tab. 4.

Table 4. The effective Young's modulus of sintered iron samples before and after eight weeks of immersion in Hank's solution.

Compaction pressure [MPa]	Effective Young's modulus [GPa]	
	Sample before immersion	Sample after immersion
100	35.8	41.3
200	64.5	68.2
400	104.4	105.3
600	133.6	134.1

As expected, the effective Young's modulus of as-sintered materials increases with increasing relative density.

It was also expected that the exposure of samples to Hank's solution would reduce the effective Young's modulus as it was observed for another kinds of sintered materials [e.g. 5].

Surprisingly, the eight-week immersion in Hank's solution raised the effective Young's modulus of investigated materials. To examine the uniformity and depth of the corrosive attack, surface layers of various thickness were removed from opposite sides of a bar-shaped sample and flexural vibrations both parallel and perpendicular to the removed surface layers were used. The value obtained for the effective modulus remained unchanged. This implies that the material is macroscopically nearly homogeneous throughout the whole after-exposure sample, that is, the corrosion affected the whole sample, not only regions beneath the surface.

A possible explanation for the observed increase in the effective Young's modulus is as follows.

The bending stiffness quantifies the resistance of a bar to elastic bending. When the bar is bent, it is stretched at some points and compressed at others. The material near the convex side of the bar resists tension, and that near the concave side resists compression. So, the resistance to bending arises from the cooperation of resistance to extension and resistance to contraction acting simultaneously. If, as usually, the modulus in tension equals that in compression, the bending stiffness is proportional to this unique modulus [13].

During the long exposure to the electrolyte, more or less cohesive layers of degradation products were adhered to and deposited on internal surfaces more or less uniformly throughout the whole sample. These layers do not significantly affect the tensile stiffness of the material. But films of corrosion products, especially those in narrow slits, could raise the material's compressive stiffness.

With different stiffness in tension and compression, the homogeneous bar undergoing bending behaves like a composite one consisting of two different materials, one represented by a stretched part of the bar, the other by its compressed part. The bending stiffness of a such homogeneous bar (and so

the Y_{eff} .) depends on two different moduli of elasticity - modulus in tension, Y_t , and modulus in compression, Y_c .

Using the relations published in papers [14, 15], the effective Young's modulus determined by means of flexural vibrations of a bar made of a material with different stiffness in tension and compression can be expressed as

$$\sqrt{\frac{1}{Y_{eff}}} = \frac{1}{2} \sqrt{\frac{1}{Y_t}} + \frac{1}{2} \sqrt{\frac{1}{Y_c}} \tag{8}$$

It is supposed that for as-sintered materials $Y_t = Y_c$, so $Y_{eff} = Y_t = Y_c$.

Regarding the materials which underwent immersion, it is supposed that Y_t did not change but Y_c increased, that is, $Y_c > Y_t$. Then, if determined by means of flexural vibrations, the effective Young's modulus of a material after exposure is expected to be higher than the Young's modulus of a material before exposure (Fig. 7).

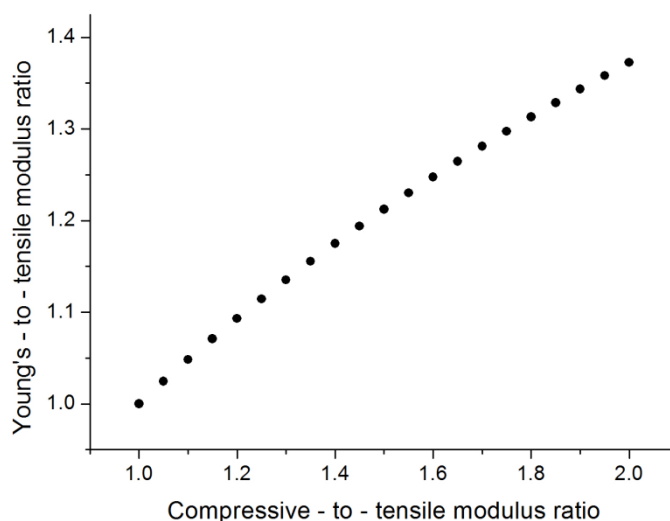


Figure 7. The effective Young's modulus reflected in the bending stiffness of a bar made of a material with different modulus in tension and compression. The data were calculated by use of relation (8).

4. CONCLUSION

Sintered iron samples were prepared with porosity ranging from 15 to 40%. As-sintered samples were brought into a contact with Hank's solution and their corrosion potentials were measured. It was found that the corrosion potential increased with decreasing porosity of samples. Such a dependence of corrosion potential on porosity is attributed to the increasing cathode-to-anode area ratio of a sample undergoing galvanic corrosion. The external surface of sintered sample acts as the cathode and the surface of internal walls of pores serves as the anode. The former surface increases and

the latter one decreases with decreasing porosity. As expected, the effective Young's modulus of as-sintered materials increased with decreasing porosity.

The samples were then immersed in Hank's solution for eight weeks. After taking out of the electrolyte, cleaning and drying, each of samples exhibited an increase in mass which was found proportional to the sample's internal surface. This is attributed to layers of corrosion products and precipitates adhered to or deposited on the internal surface. Due to non-spherical shapes of pores and the volume fraction which the pores occupy, investigated samples are considered to be permeable for liquids. This enables Hank's solution to fill almost all void spaces of the sample and, as the time passes, to cover the internal surface of pores with a more or less uniform layer of reaction products.

Surprisingly, after the eight-week exposure of samples to Hank's solution, the effective Young's modulus of each sample was higher than in its as-sintered state, and neither the polarization of used flexural vibration nor the removal of surface layers of various thickness did affect the modulus value. This is attributed to a possible increase in the compressive stiffness of the material due to the presence of films of corrosion products in narrow slit-like pores throughout the whole sample. Though the tensile stiffness remains unchanged, enhanced compressive stiffness leads to a higher bending stiffness, thus to a higher natural frequency of flexural vibration and hence to a higher evaluated value of the effective Young's modulus.

Unlike as-sintered samples, the samples which underwent immersion in Hank's solution had nearly identical corrosion potentials irrespective of different porosities. This implies the occurrence of a general corrosion.

The choice of phenomena and processes, which are expected to underlie the observed behaviour of sintered iron materials, need to be justified by an additional, more targeted study. This represent the goal for further investigation.

ACKNOWLEDGEMENTS

The authors thank for financial support of the research by the Slovak Research and Development Agency under contract APVV No. 0677-11 and VEGA grant 2/0100/15.

References

1. R. German, *Sintering: from empirical observations to scientific principles*, Elsevier Butterworth-Heinemann, (2014) Oxford, UK.
2. A. Bautista, F. Velasco, S. Guzmán, D. De la Fuente, F. Cayuela and M. Morcillo, *Rev. Metal.*, 42 (2006) 175.
3. E. Klar and P. K. Samal, *Powder metallurgy stainless steels: processing, microstructures, and properties*, ASM international, (2007) Materials Park, OH.
4. J. A. Cabral-Miramontes, J. D. O. Barceinas-Sanchez, C. A. Poblano-Salas, G. K. Pedraza-Basulto, D. Nieves-Mendoza, P. C. Zambrano-Robledo, F. Almeraya-Calderón and J. G. Chacón-Nava, *Int. J. Electrochem. Sci.*, 8 (2013) 564.
5. M. Kupková, M. Hrubovčáková and M. Kupka, *Mater. Sci. Forum*, 844 (2016) 46.
6. J. P. Jernot, M. Coster and J. L. Chermant, *Powder Technol.*, 30 (1981) 21.
7. E. J. Garboczi, K. A. Snyder, J. F. Douglas and M. F. Thorpe, *Phys. Rev. E*, 52 (1995) 819.
8. Y. B. Yi and A. M. Sastry, *Proc. R. Soc. London, Ser. A*, 460 (2004), 2353.

9. H. Hermawan, A. Purnama, D. Dube, J. Couet and D. Mantovani, *Acta Biomater.*, 6 (2010) 1852.
10. Q. Zhang and P. Cao, *Mater. Chem. Phys.*, 163 (2015) 394.
11. Y. H. Yau and M. A. Streicher, *Corrosion*, 43 (1987) 366.
12. J. R. Nimmo, Porosity and pore size distribution. *Encyclopedia of Soils in the Environment*, 3 (2004) 95.
13. L. D. Landau and E. M. Lifshitz, *Theory of Elasticity*. 2nd. English Edn., Pergamon, (1970) Oxford, UK.
14. M. Kupka and M. Kupková, *J. Phys. D: Appl. Phys.*, 34 (2001) 232.
15. M. Kupka and M. Kupková, *J. Phys. D: Appl. Phys.*, 39 (2006) 4097.

© 2017 The Authors. Published by ESG (www.electrochemsci.org). This article is an open access article distributed under the terms and conditions of the Creative Commons Attribution license (<http://creativecommons.org/licenses/by/4.0/>).